HAL
open science

Hydrogel Matrix Grafted Impedimetric Aptasensor for the Detection of Diclofenac

Getnet S Kassahun, Sophie Griveau, Sophie Juillard, Joffrey Champavert, Armelle Ringuede, Bruno Bresson, Yvette Tran, Fethi Bedioui, Cyrine Slim

To cite this version:

Getnet S Kassahun, Sophie Griveau, Sophie Juillard, Joffrey Champavert, Armelle Ringuede, et al.. Hydrogel Matrix Grafted Impedimetric Aptasensor for the Detection of Diclofenac. Langmuir, 2020, 36, pp.827 - 836. 10.1021/acs.langmuir.9b02031 . hal-02433456

HAL Id: hal-02433456

https://hal.science/hal-02433456v1

Submitted on 9 Jan 2020

HAL is a multi-disciplinary open access archive for the deposit and dissemination of scientific research documents, whether they are published or not. The documents may come from teaching and research institutions in France or abroad, or from public or private research centers.

L'archive ouverte pluridisciplinaire **HAL**, est destinée au dépôt et à la diffusion de documents scientifiques de niveau recherche, publiés ou non, émanant des établissements d'enseignement et de recherche français ou étrangers, des laboratoires publics ou privés.

Hydrogel Matrix Grafted Impedimetric Aptasensor for the Detection of Diclofenac

G. S. Kassahun[a], S. Griveau[a], S. Juillard[a], J. Champavert[a], A. Ringuedé[c], B. Bresson[b], Y. Tran[b], F. Bedioui[a], C. Slim*[a]*

[a] Institute of Chemistry for life and health sciences (iCLeHS), PSL Research University, CNRS, Chimie ParisTech, 11 rue Pierre et Marie Curie, 75231 Paris Cedex 05, France

[b] Soft Matter Engineering and Science, PSL Research University, UMR 7615 CNRS, ESPCI, 10 rue Vauquelin, F-75231 Paris Cedex 05, France

[c] Institut de Recherche de Chimie de Paris (IRCP), PSL Research University, CNRS, Chimie ParisTech, 11 rue Pierre et Marie Curie, 75231 Paris Cedex 05, France

Corresponding Authors:
cyrine.slim@chimieparistech.psl.eu

yvette.tran@espci.fr

ABSTRACT

Driven by the growing concern about the release of the untreated emerging pollutants and the need for determining small amount of these pollutants present in the environment, novel biosensors dedicated to molecular recognition are developed. We have designed biosensors using a novel class of grafted polymers, surface-attached hydrogel thin films on conductive transducer as a biocompatible matrix for biomolecule immobilization. We showed that they can be dedicated to the molecular recognition of Diclofenac (DCL). The immobilization of the aptamer onto surface-attached hydrogel thin films by covalent attachment provides a biodegradable shelter, providing the aptamer excellent environments to preserve its active and functional structure while allowing the detection of DCL. The grafting of the aptamer is obtained using the formation of amide bonds *via* the activation of carboxylic acid groups of the poly (acrylic acid) (PAA) hydrogel thin film. For improved sensitivity and higher stability of the sensor, a high density of immobilized aptamer is enabled. The aptamer modified electrode was then incubated with DCL solutions at different concentrations. The performances of the aptasensor

were investigated by Electrochemical Impedance Spectroscopy (EIS). The change in charge-transfer resistance (Rct) was found to be linear with DCL concentration in the 30 pM – 1 μM range. The detection limit was calculated to be 0.02 nM. The improvement of the limit of detection can be mainly attributed to the three-dimensional environment of the hydrogel matrix which improves the grafting density of aptamer and the affinity of the aptamer to DCL.

Keywords: Aptamer; Electrochemical Biosensors; Impedimetric aptasensors; Diclofenac; Emerging pollutants; Hydrogel

INTRODUCTION

The detection of drug residues as contaminants in water and food is of high importance in the fields of human health and environment. One of the commonly used drugs is Diclofenac (DCL), or 2-(2-((2,6-dichlorophenyl)amino) phenyl)acetic acid, marketed with the trade name Voltaren®. This drug is a nonsteroidal anti-inflammatory drug (NSAID) prescribed for its anti-inflammatory, analgesic, and antipyretic properties [1] to treat inflammatory joint diseases and mild to moderate pain [3,4]. Because of its frequent use, DCL residues have often been detected in freshwater environments [5-7]. DCL also belongs to the list of emerging pollutants (EP) because of the risk it may presents for health and environment [8,9]. There is currently a large list of EPs substances, as drugs (antibiotics, pharmaceuticals, hormones), products for daily use (detergents, disinfectants, antioxidants…) and products of industrial origin (flame retardants, nanoparticles) characterized by a wide distribution in the environment due to their massive daily use and persistence [10,11]. EPs are commonly present at trace concentrations and characterized by their long-term health effects, such as nervous system damage, toxicity or cancer appearance due to their accumulation and persistence, even at very low concentrations [12]. Many studies have described the potential effects of DCL on organisms when exposed to environmental

levels ranging from a few ng L^{-1} to tens of µg L^{-1} in surface water [13,14,15].

On the light of concerns about possible adverse effects of DCL on organisms and on aquatic life, its essential to quantify this drug in environmental waters, not only to assess accurately its environmental risk and characterize the dangers due to its environmental exposure but also to verify and improve the efficiency of wastewater treatment processes [16]. Until now, its detection essentially depend on conventional techniques, such as HPLC [17,18] and GC/MS [19]. Although these analytic techniques are very robust, they are expensive, time consuming, require experts and are not portable in the field. Electrochemical methods are an attractive alternative for the analysis of pharmaceutical, biological and environmental compounds. They provide many benefits over thermal, optical and piezoelectric detection including ease of use, rapidity, cost-effectiveness, high sensitivity and selectivity, ease of miniaturization, compatibility with novel micro-fabrication technologies and robustness [20-29]. Electrochemical reactions generally produce an electronic signal directly, without the the need of expensive signal transduction equipment.

Various electrochemical methods have been reported for the determination of DCL such as amperometric [30-33] and potentiometric techniques [24, 34-36]. Modified electrodes comprising Cu-doped

zeolite-expanded graphite-epoxy electrode [37], graphene or carbon nanotubes [38,39] have been also used. For improving the limit of detection (LOD), biomolecules that are specific for the DCL have been utilized by using antibodies also [40,41].

When it comes to electrochemical sensing, aptamer based biosensors (aptasensors) are promising tools, which take advantages of the use of aptamers as probes in order to detect specific targets [42]. Aptamer are single-stranded DNA (ssDNA) or RNA molecules able to bind target molecules with high affinity [43]. Because of their specific binding abilities and many advantages over antibodies including their higher stability, lower cost, specificity and affinity [44-47], their easy reliable production [44,45], their easy chemical modification offering diverse immobilization ways [50], their easy regenerability [46,48] and their storability [46,49], they provide a great opportunity to produce sensing surfaces for effective and selective electrochemical detection of harmful small molecules such as DCL and their real-time monitoring in the environments [51]. Among the different electrochemical detection techniques, electrochemical impedance spectroscopy (EIS) has emerged as appealing strategy [52,53].

Studies on detection of DCL using aptasensors are rarely described to our knowledge, and recently a very few EIS aptasensors have been built based on the interfacial property [29,54].

In this work, we have developed a novel aptasensor for DCL. To this end, a new class of surface-attached hydrogel thin films was grafted on conductive transducer and used as biocompatible matrix for aptamer immobilization, tuned for the conception of biosensor. The polymeric network environment favors the stable immobilization of the aptamer and the selective affinity to the target and sensitive electrochemical detection, by providing the aptamer excellent environments to preserve its active and functional structure [55]. Surface-attached hydrogel thin films present then many advantages as immobilization matrix: they are stable, robust, multiscale and multifunctional materials, with different thickness ranges from a few nanometers to several micrometers. The deformability, permeability and porosity of the hydrogel films can also be easily and finely adjusted with the film thickness and the network crosslinks density.

The synthesis of reproductible and reliable hydrogels films was produced using a simple and versatile approach, the Cross-Linking And Grafting process (CLAG). It consists of using thiol-ene click chemistry to preform functionalized polymers. As described by Chollet *et al.* [56] the advantages of the synthesis of the preformed reactive polymers chains consist of avoiding the constraint of working under a controlled atmosphere due to the oxygen inhibition of radical polymerization. This versatile approach allows then easy adjustment of the chemical properties (platform for covalent

immobilization) and physical properties (size and architecture) hydrogel films.

EXPERIMENTAL SECTION

Chemicals

Poly(acrylic acid) (PAA) (M_W ~ 250 kg/mol, 35 wt% solution in water), allylamine, N-hydroxysuccinimide (NHS), 1-ethyl-3-(3-dimethylaminopropyl) carbodiimide (EDC), 1,4-dithioerythritol (DTE), diclofenac (DCL), potassium ferricyanide [$K_3Fe(CN)_6$], potassium ferricyanide [$K_4Fe(CN)_6$], and potassium/sodium phosphate monobasic/dibasic were purchased from Sigma-Aldrich and were used as received. Chloroform, methanol, formic acid solvents were also purchased from Sigma-Aldrich.

The aptamer used for sensing (amine terminated fluorescently labeled DCL aptamer (75 bases)) had the 5'-/5AmMC6/ATA CCA GCT TAT TCA ATT GCA ACG TGG CGG TCA GTC AGC GGG TGG TGG GTT CGG TCC AGA TAG TAA GTG CAA TCT/36-FAM/-3' sequence and was purchased from Integrated DNA technologies.

The aptamer solution was prepared using a phosphate buffer solution (0.1 M, pH 7.4). The working aptamer solutions were prepared from a 100 µM aptamer stock solution by diluting to the desired final concentration. The aptamer stock solution was prepared and stored at −20 °C.

Other chemicals used were of analytical grade and have been used as supplied. Deionized water (18.2 MΩ/cm) purified using a Pure Labflex system (Elga Water, Veolia, France) was used throughout the experiment for aqueous solution preparation.

For the determination of DCL in water sample, a stock solution of 100 mM DCL was daily prepared, and was then diluted at different concentrations using 200 µL binding washing buffer (BWB) (10 mM NaCl, 0.5 mM KCl, 0.2 mM $MgCl_2$, 0.1 mM $CaCl_2$ and 5% ethanol in 2 mM Tris-HCl at pH 7.5).

Characterization of the biosensor

EIS measurements

We used a conventional three-electrode cell. A Saturated Calomel reference Electrode (SCE), a platinum wire as counter electrode and a modified gold working electrode. A Bio-Logic instrument (Bio-Logic SP-300) equipped with EC-Lab software was used to carry out all the cyclic voltammograms and EIS measurements. EIS measurements were performed with a potential equal to 0 V (relative to the OCP), over the frequency range of 10 kHz to 1 mHz with an oscillation potential of 10 mV. Cyclic voltammograms and impedance measurements were carried out in the presence of a mixture of $K_3[Fe(CN)_6]/K_4[Fe(CN)_6]$ at 5 mM, in PBS (0.1 M at pH 7.4).

Atomic Force Microscopy

The gold electrode and the PAA hydrogel functionalized electrodes were also characterized by AFM. A Bruker ICON microscope controlled by a Nanoscope V was used for the acquisition of all the images. The thickness of the gold electrode and the PAA hydrogel is determined at the edge of the pattern. The height images of the

gold surface and the films of hydrogel in air were obtained in tapping mode at 300 kHz with a standard tip of stiffness 40 N/m. The half width of the height distribution histogram extracted from the images defines the roughness. The imaging conditions for very soft gel in water have been discussed in details by Li *et al.* [57]. As very soft matter is probed, a tip with a lower stiffness is preferred if the adhesion is not preponderant. In our case, a compromise is chosen with a typical contact tip with a stiffness of 0.2 N/m.

The Peak Force mode is preferred to probe hydrogel films in water when imaging soft matter in water. In this mode, the probe and the sample are intermittently brought into contact for a short period and can be considered as a succession of approach-retract curves performed at high frequency (1 kHz) and limited by a maximum set force which can be finely tuned. This mode allows to reduce the lateral and shear forces during the scanning. A cantilever of stiffness of 0.7 N/m, with a typical Force Set Point of 1nN was used to obtain the Peak Forces images in water. The amplitude of the tapping was about 200 nm. The size of the images is 1 μm.

Other characterization techniques

ATR-FTIR was performed in Agilent Cary 660. The water contact angle measurements of the different stages of electrode fabrication was obtained by dropping a drop of water and using the KRUSS drop shape analyzer with the Sessile Drop method.

The secondary electron imaging of the different stages of construction was done using FEI Thermo Fischer Magellan SEM equipped with a FEG source.

Target Detection

Detection of DCL were carried out by incubating the aptasensor in 200 µL BWB solution containing DCL for 50 min at room temperature. After detection, the non-bound molecules of DCLwas removed by washing three times the electrode with BWB solution.

Construction of the aptasensor

The subsequent steps of manufacturing the aptamer based electrochemical sensor undergone in this study are illustrated in Scheme 1. It consists in preparing the gold electrode with positive lithography (A) (see Figure S1, supporing information), modifying the gold electrode with dithiol molecules (B) and simultaneously CLAG ene-functionalized PAA by thiol-ene click reaction to form hydrogel surface-attached matrix (C). The steps are detailed below.

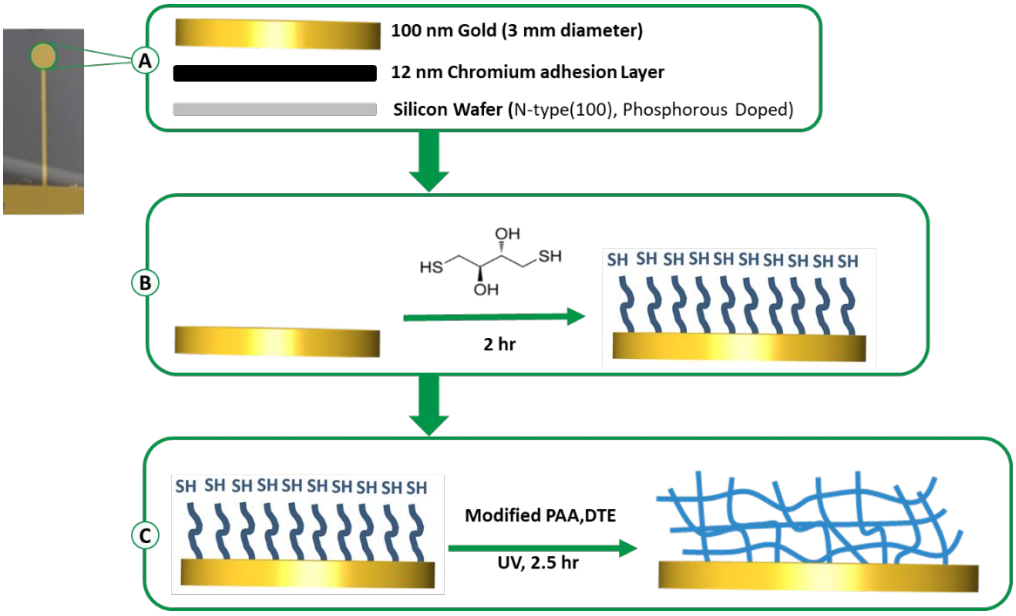

Scheme 1: Different steps of aptasensors construction ;(A) gold electrode made by positive photolithography; (B) thiol modification of the gold electrode; (C) hydrogel grafting using thiol-ene click chemistry.

Preparation and thiol-functionalization of gold electrode transducer

First, the transducer was prepared, as a thin layer gold electrode deposited on silicon wafer. To this end, evaporated gold films were obtained using N-type phosphorous doped silicon wafer with 100 orientations (resistivity: 1-20 ohm.cm) as substrate . To promote adhesion and cleanliness, the silicon wafers were cleaned by oxygen plasma prior to coating. A positive photolithography process was used to prepare the thin layers by thermal evaporation of ~100 nm gold onto a ~12 nm chromium adhesion layer.

The gold thin film working electrode, with a diameter of 3 mm, were subsequently cleaned in 50 mM KOH and 25 % H_2O_2 for 30 minutes. The electrodes were then characterized by cyclic voltammetry at 50 mV/s in $K_3[Fe(CN)_6]$ aqueous solution to check the reversibility of redox couple and compare experimental to theoretical peak currents (see Figure S2, supporting information).

The functionalization of the activated gold surfaces with thiol self-assembled monolayers was carry out using a solution of 1 mM dithioerythritol (DTE) in chloroform for 2 hours. The thiol-modified surfaces were then rinsed and sonicated in chloroform and dried with nitrogen flow.

Hydrogels grafting on gold electrodes

Poly(acrylic acid) hydrogel chains were randomly functionalized with ene-groups at their carboxylic acid sites. Allylamine was graft onto polymer chains using a peptide reaction in the presence of EDC as the dehydration agent and NHS as the addition agent to increase yields and decrease side reactions [58]. Briefly, a 20 wt % solution of PAA in Milli-Q water at a pH of 4.5 was mixed with NHS and EDS for 2 hours at 60 °C. Allylamine was then added (the molar ratio AA/allylamine/EDC/NHS being set equal to 10/1/1.5/1.5) and the pH was adjusted to 10 before the reaction was allowed to proceed for 16 hours at 60°C. After 3 days of dialysis in 0.1 M

NaCl solution and 3 days of dialysis in Milli-Q water, the polymer was finally recovered through freeze-drying

PAA hydrogel thin films were synthesized on the electrode surface by simultaneously cross-linking and grafting preformed polymer chains through thiol–ene click chemistry strategy as reported by Chollet *et al.* [56] and Li *et al.* [57]. More precisely, the ene-functionalized PAA polymer (0.5 wt %) was dissolved in the methanol and formic acid mixture 7:3 (V/V) and the solution was stirred for one night. The coatings were carry out by spin-coating of the ene-functionalized polymer solution on thiol-functionalized gold electrodes, with the addition of dithiol cross-linkers at 3000 rpm for 30 seconds.

Aluminum foil were used as a mask for patterning. The CLAG were simultaneously obtained by exposing the assembly to UV irradiation at 254 nm for 2.5 hours. The electrode was then rinsed in methanol using ultrasonic bath for 1 minute and then dried with N_2 flow. We obtained homogeneous hydrogel thin films with well-controlled thickness with a dry thickness being about 57 nm.

Immobilization of aptamer on hydrogel-modified transducer

The covalent grafting of the amino-labeled aptamer solution on the resulting Poly(acrylic acid) hydrogel modified electrode was performed by using *in situ* two-step attachment method. The modified electrode was incubated for 30 minutes at 20°C in phosphate buffer of pH 6.2 containing 50 mM EDC and 100 mM NHS. The electrode was

subsequently rinsed with phosphate buffer (pH 7.4) and then incubated with 10 μM aptamer in phosphate buffer solution of pH 7.4 for 1 h at 20°C. Before grafting, the aptamer solution was heated at 75°C for 5 min. Once the grafting of the aptamer have been done, the electrode was washed with a phosphate buffer solution to remove the unreacted aptamer.

RESULTS AND DISCUSSION

Topography and thickness of electrode-attached hydrogel films

For the different stages of electrode construction, contact angle measurements were performed to evaluate the presence of the different layers put on and hence (see figure 1), the same is confirmed by analyzing the materials hydrophobicity and/or hydrophilicity. Though the water contact angle (WCA) value shows relatively a hydrophobic surface for the silicon wafer, after the plasma cleaning the wafer exhibited dramatic differences in the contact angle indicating the surface change from a hydrophobic state to hydrophilic. The WCA of the gold (~62°) indicated that the material does not have a hydrophilic character.

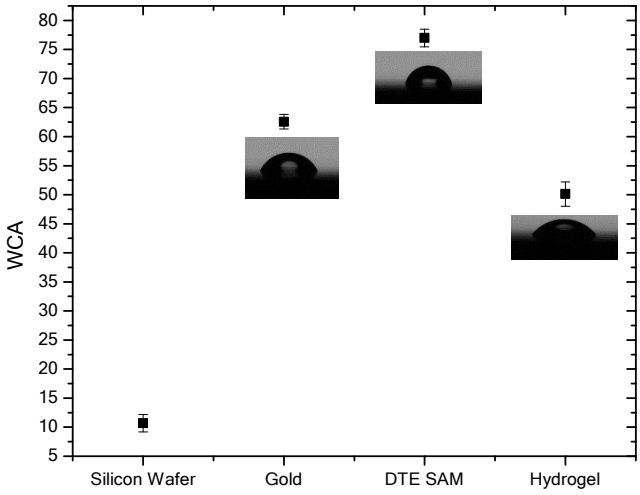

Figure 1. Water contact angle of the different stages of electrode fabrication

The WCA on the DTE SAM exhibited distinctly higher contact angles (~75°) compared to that of the clean gold electrode, evidencing the modification of gold surface properties. WCA measurements of SAMs is reported to have a parity (or odd-even) *vs* chain-length relationship [59,60].

After the formation of PAA hydrogel on thiol-modified gold electrode, the water contact angle is around 50°. Accounting for the homogeneity and smoothness of the thin film, the contact angle expresses the presence of polymeric polyelectrolyte surface and this result is consistent with a study described for the water contact angle of hydrophilic and negatively charged hydrogel at constant grafting density [61].

The thickness of both the gold and hydrogel layer grafted on a DTE SAM-modified gold substrate was determined using AFM measurements (Figure 2). It was found to be around 100 nm for the bare gold electrode and 57 nm for the PAA hydrogel. The dry thickness of the PAA hydrogel film is consistent with the value found by our group for surface-attached hydrogel films using spin-coated polymer solution with concentration of 0.5 wt % and molecular weight of 250 kg mol^{-1} [56].

The swelling ratio measured as the ratio of the swollen thickness of hydrogel films (measured in water) to the dry thickness (measured in air) was found to be 1.8. It was obtained for the hydrogel films fabricated with 2 % ene-reactive groups and 30 times the ene-reactive groups excess of dithioerythritol cross-linkers. This result is consistent with the study that states for thin films less than 150 nm, the swelling rate increases with the thickness of the film and it is independent of the thickness in the range of 150 nm to a few micrometers [56,57]. This is related to the strong effect that the surface grafting has on the swelling of the films. Due to this constraint of surface attachment nanometric hydrogel films swell on average less than micrometric layers.

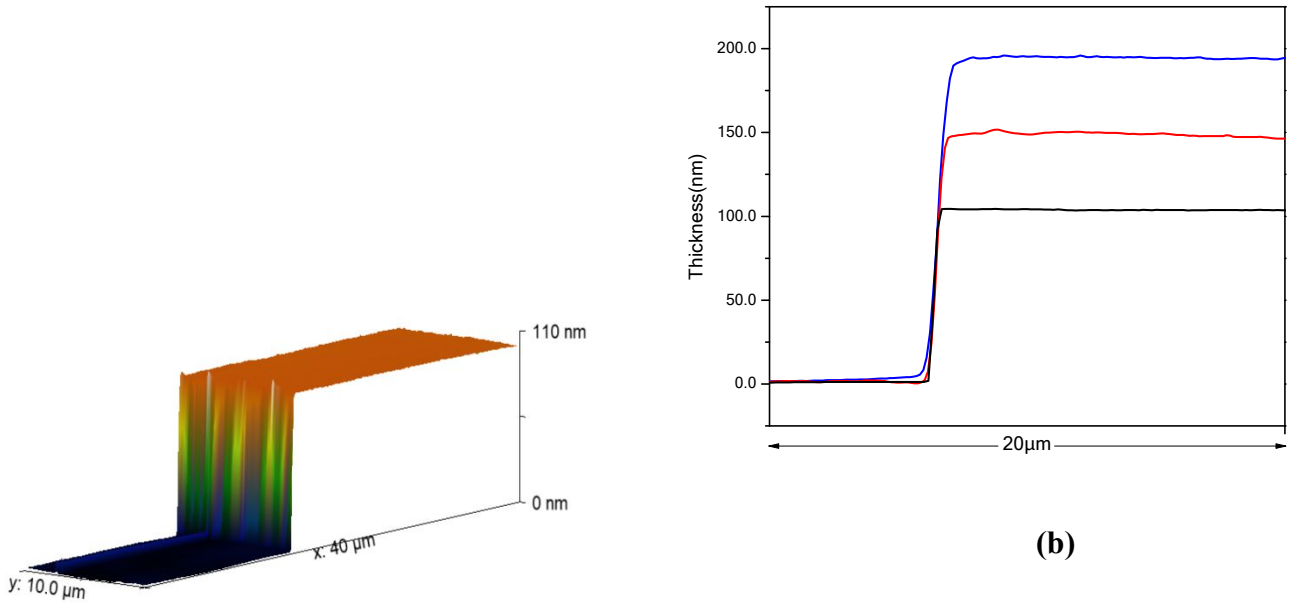

(a) (b)

Figure 2. (a) Schematics of height profiles obtained by AFM for bare gold. (b) Height profiles of gold electrode (in black), PAA hydrogel film in air (red) and PAA hydrogel film in water (blue).

Topographic images and height profiles of the bare gold surface, the surface-attached hydrogel film in air and the surface attached hydrogel immersed in water have been determined by AFM (Figure 3 and Figure S3 in the supporting information) and scanning electron microscopy (SEM) (Figure 4 and Figure S4 (Supporting Information)). The height image obtained from the evaporated gold surface shows a typical grainy structure (Figure 3a). To illustrate the roughness difference between the samples on Figure 3, a profile line is extracted for each height image and displayed beyond the image. The roughness of the gold surface can be extracted from the

AFM images measuring the half width of the height histogram of the image. From the Figure 3 (a), a roughness of 4 nm is obtained. Moreover, the same value (~ 4 nm) is obtained for both images (1 μm- and 10 μm-scales), proving that the roughness is independent of the size of the sample and is homogeneous. In the general case, the roughness strongly depends on the image size, but here, the roughness of the sample is completely determined by the morphology of the coated gold on the (plane) silicon wafer. It means that increasing the image size does not reveal additional lower spatial frequency. All in all, the large homogeneity of the bare gold electrode at 10 μm-scale and the granular structure at 1 μm-scale observed by AFM are also confirmed by SEM (Figure 4).

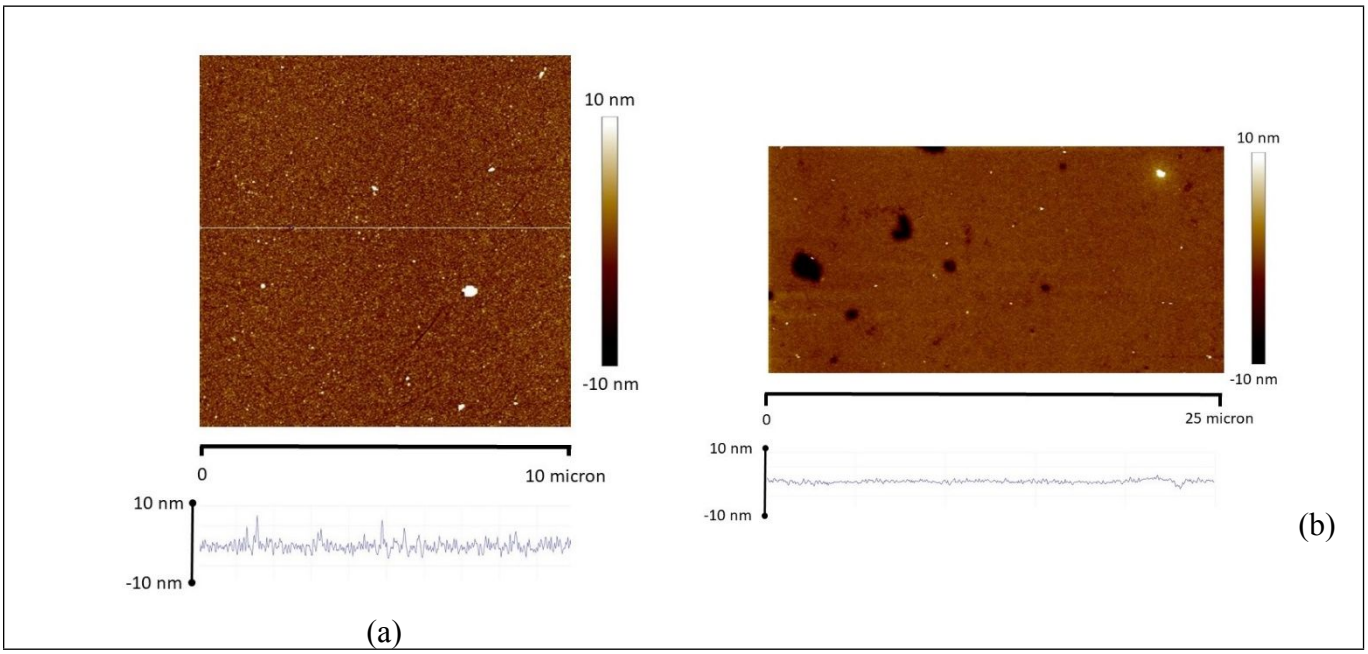

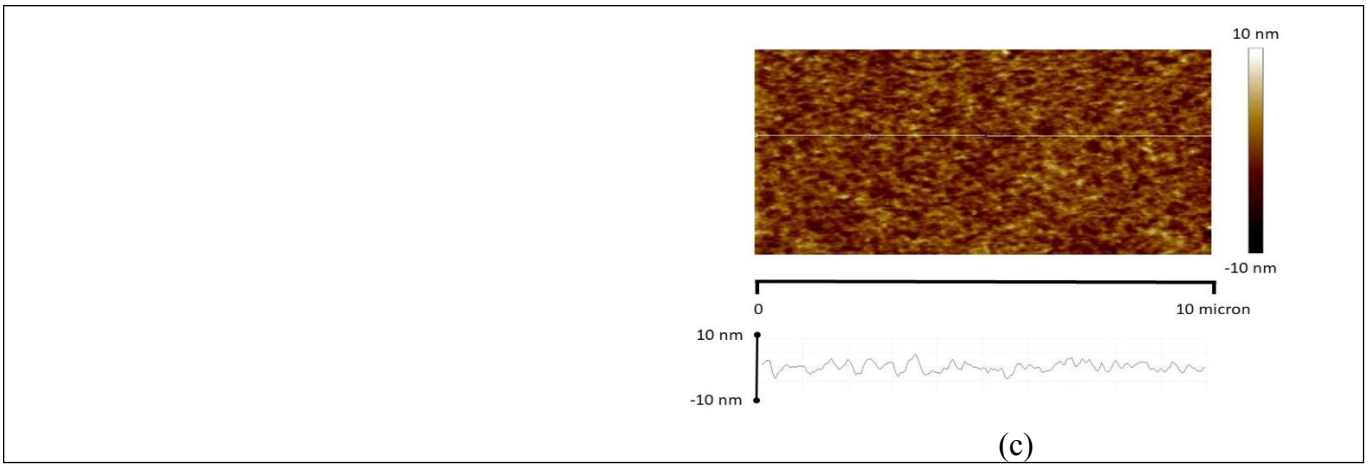

Figure 3. AFM tapping height images of the bare gold electrode surface (a), AFM tapping height images of the hydrogel film in air (b) and AFM height contact images of the hydrogel film immersed in water (c).

The AFM images of PAA hydrogel film in air (Figure 3b) also show that the roughness, estimated to 1 nm (half width of the height histogram of the image), is homogeneous. Even though the thickness of the hydrogel film (~ 57 nm) is much higher than the roughness, the surface of the hydrogel film replicates that of the gold electrode and follows strictly the same granular structure. The replication of the morphology of gold surface is clearly confirmed by SEM. In Figure 5, the SEM image displays the frontier between the hydrogel film (dark region) and the bare gold surface. The inset enables to highlight the granular structure on both surfaces of the gold electrode and the hydrogel film with a slightly lower topography contrast in the hydrogel region. The fine observation of the hydrogel region (upper part of the Figure 5) on the large

(50 μm-) scale confirms the high planarity of the hydrogel surface. Finally, the hydrogel film immersed in water (Figure 3c) showed higher roughness (~ 4 nm) than that in air, as the gel swells (the swelling ratio is 1.8).

As a result, we show that the roughness of the hydrogel film surface is due to the replication of the granular morphology of the gold electrode. It is anyway much lower than the thickness of the layer, so that the hydrogel film can be considered as fully homogeneous and plane. From the measure of the dry thickness (h = 57 nm) and the swelling ratio (S = 1.8), we can calculate the concentrations of acrylic acid unit. The volume concentration C_V can be calculated by: $C_V = \rho / (S \mathrm{x} M)$ where is the density of poly(acrylic acid) and M is the molecular weight of acrylic acid unit. The surface concentration C_S is calculated by: $C_S = (h \mathrm{x} \rho) / M$. We obtained $C_V = 8\ 10^{-3}$ mol/L and $C_s = 0.82\ 10^{-9}$ mol/m^2.

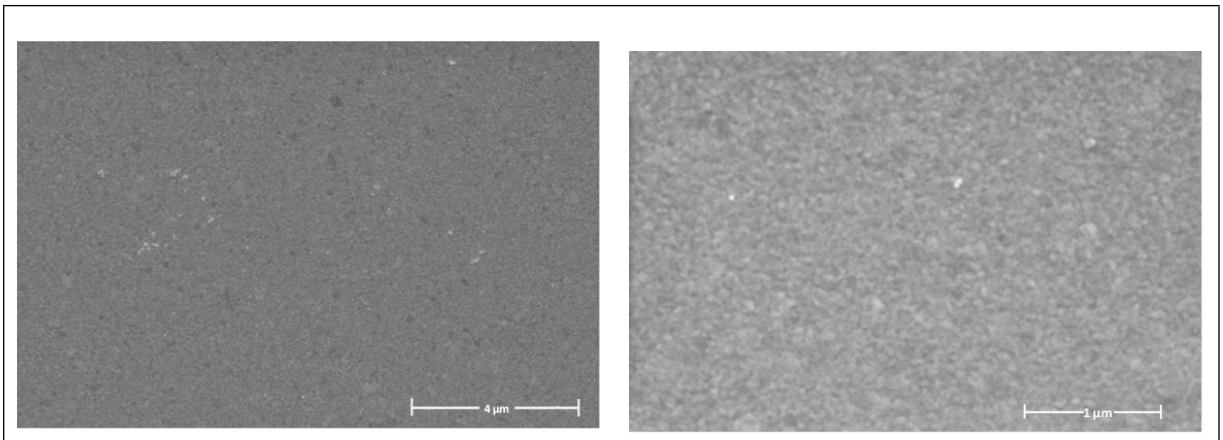

Figure 4. SEM images of the bare gold electrode surface at different scales

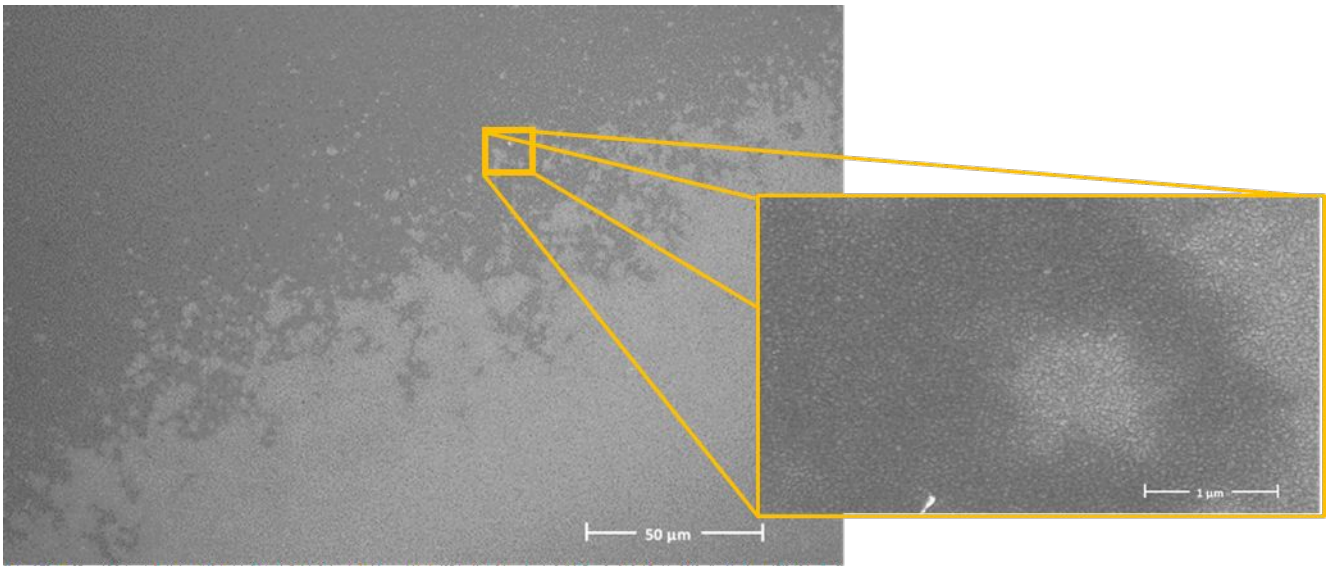

Figure 5. Surface morphology of hydrogel (dark area) and gold (white area) visualized using scanning electron microscope (SEM)

Characterization of the hydrogel-modified electrode

Electrodes were also characterized by ATR-FTIR spectroscopy and electrochemistry, after cross-linking and grafting of PAA to evidence the presence of the hydrogel on the electrode surface. Figure 6 shows the ATR-FTIR spectra between 500 and 4000 cm^{-1} of the gold electrode after thiol modification and the formation of PAA hydrogel. As the contact between the ATR-diamond waveguide and the solid silicon substrate cannot be reproducible for different samples, the absorbance is in arbitrary unit. This representation also enables to highlight the absorption bands. The spectrum (a) clearly demonstrates that the gold electrode is modified by thiol molecules. First, the covalent gold-sulfur bond is proven by the presence of the large band in the range of 500 to 750 cm^{-1}, which

can be attributed to the stretch mode of C-S bond. Second, the vibration mode of alkyl thiol is observed at 2917 cm^{-1}. Moreover, the peaks at 1017 cm^{-1} correspond to the O-H deformation mode. The O-H stretching vibrations in the range of 3100-3500 cm^{-1} can also be clearly seen.

The FTIR-ATR spectrum (b) is obtained with the gold electrode modified by the PAA hydrogel. It evidences the O-H stretching band in 3400 cm^{-1} region and the CH_2 (asymmetric) stretching at 2925 cm^{-1}. Also, the bands at 1700 cm^{-1} are attributed to C=O stretching band of PAA. Comparing spectra (a) and (b), it could be noticed that the O-H stretching vibration in the range of 3100 – 3500 cm^{-1} is different. The absorption band of the PAA hydrogel which is characteristics of hygroscopic compound is broader due to the presence of H-bonds (in comparison with the O-H stretching band of thiol monolayer). The decrease of the O-H band at 1017 cm^{-1} is due to the arbitrary unit of the absorbance. Finally, it should be noted that the presence of C-S band in PAA hydrogel spectrum is not surprising as the thickness of the hydrogel film is much less than the penetration depth of the evanescent wave of the ATR-infrared beam (a few microns).

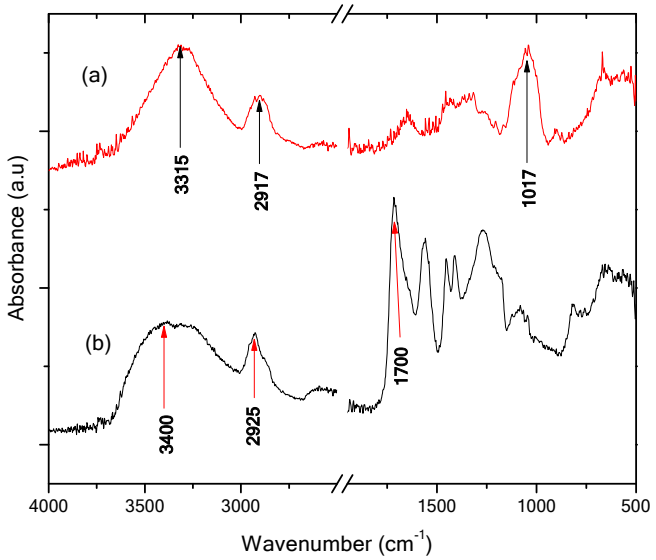

Figure 6. FTIR-ATR spectra of thiolated gold electrode (a) and PAA hydrogel grafted gold electrode (b).

The PAA hydrogel modified electrode was also electrochemically analyzed by cyclic voltammetry. Figure 7 shows the voltammograms of $Fe(CN)_6^{3-/4-}$ of the gold electrode at different steps of the hydrogel film preparation: bare gold electrode, thiol monolayer and PAA hydrogel film.

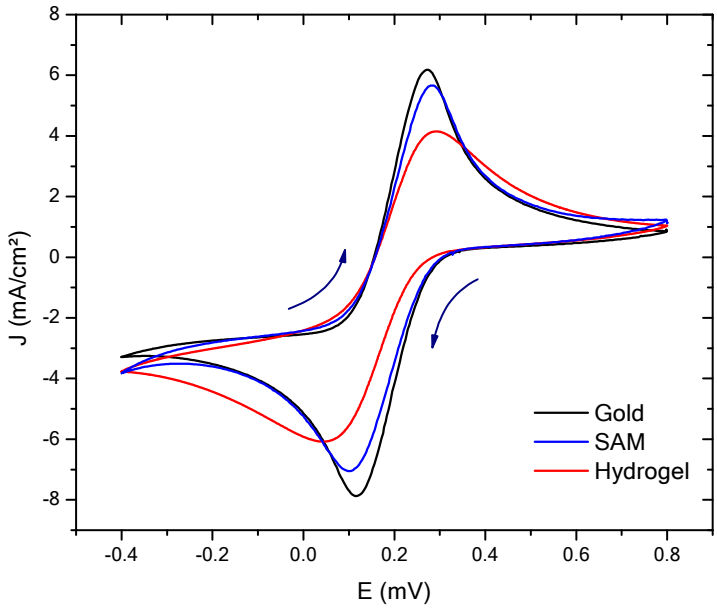

Figure 7. Characterization of the sensing interface by cyclic voltammetry at 50 mV.s^{-1} in a solution of KCl 0.1 M containing 5 10^{-2} M $K_4[Fe(CN)_6]$ and $K_3[Fe(CN)_6]$: bare gold electrode (black), thiol monolayer (blue), PAA hydrogel film (red).

The voltammogram of $Fe(CN)_6^{3-/4-}$ obtained with thiol-modified electrode is almost similar to that observed at bare gold electrode. This is attributed to the fact that the thiol molecules form a non-dense monolayer [62]. The introduction of terminal groups (−SH, −COOH, −OH, $-NH_2$) instead of the $-CH_3$ group usually results in a decrease in self-assembled ordering [63]. Thus, the monolayer of DTE thiol small molecule on gold is too thin to effectively block electron transfer on a gold surface.

At relatively high pH for which the PAA hydrogel is swollen and dissociated, when comes in contact with the negative redox probe, $Fe(CN)_6^{3-/4-}$, it causes electrostatic repulsion which will affect the interfacial electron-transfer rate of the probe and a decrease in peak current and increased separation potential in comparison to the bare gold and thiol-modified electrodes. Moreover, this can be explained with the study that describes that at low pH, polyacid brushes are fully protonated and adopt a conformation similar to that of neutral brushes [64]. At high pH, the polyacid brushes become dissociated and the brush adopt an extended polyelectrolyte brush conformation similar to that of the osmotic or Pincus regime [65].

Functionalization and Immobilization of the Aptamer

The covalent immobilization of the aptamer on the surface of the PAA hydrogel film grafted on the underlying electrode was achieved through two stages EDC/NHS chemistry. Figure 8 shows the ATR-FTIR spectra at different stages of the sensor construction: the PAA hydrogel, the activated PAA hydrogel and the grafting of the aptamer. The spectrum of the activated hydrogel shows three characteristic bands at 1815, 1790, and 1750 cm^{-1} which are representative of the carbonyl stretch modes in the COO-NHS ester moiety. After aptamer immobilization, the anhydride and NHS ester peaks disappear and new amide bands appear around 1580 cm^{-1} and

1660 cm^{-1} (characteristics of amide I and amide II), thus confirming the grafting.

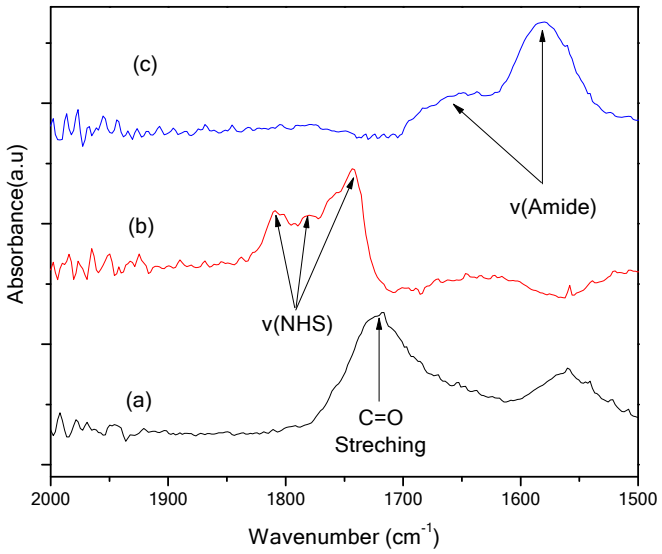

Figure 8. ATR-FTIR spectra of Au/PAA hydrogel (a), Au/activated PAA hydrogel (b) and Au/PAA hydrogel/grafted DCL aptamer (c).

Figure 9 shows the Nyquist diagrams obtained after each construction steps. The Nyquist plots of the electrodes include a semi-circle at the highest frequency range explored, and linear portion at the lowest frequencies. The semicircle is related to charge transfer resistance (Rct). The linear part is not affected by the aptasensors construction and is ascribed to diffusion processes. The variation in the Rct value is explained by the blocking effect of the step-by-step modification procedure of the electrode. The double-layer capacitance (Cdl) and Rct are

parameters relating to the dielectric and insulating properties at the electrode/electrolyte interface. These parameters are affected by variations occurring on the electrode surfaces [66].

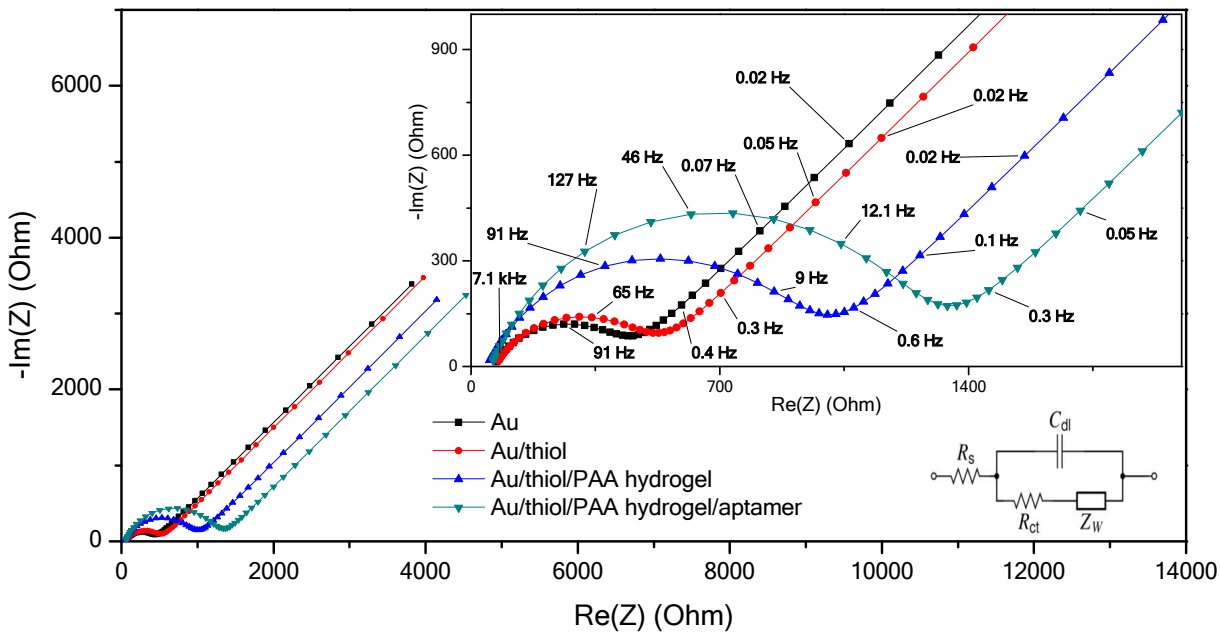

Figure 9. Nyquist plots of Au (■), Au/thiol (●), Au/thiol/PAA hydrogel (▲), Au/thiol/PAA hydrogel/aptamer (▼) electrodes in 0.1 M PBS containing 5 mM $K_4[Fe(CN)_6]$ and $K_3[Fe(CN)_6]$ in the frequency range of 10 kHz to 0.1 Hz.

When the gold electrode surface is modified using DTE layer, the Rct value slightly increased (451 ohm). There is no very significant difference, in contrary to the insulator property of thiol self-assembled monolayer. This is due to the dithiol short chain used in this study as it has been discussed during cyclic voltammetry study. In contrast, when the electrode is grafted by PAA hydrogel film, because of repulsive interaction occurring

between the negatively charged PAA hydrogel and anionic redox probe, the Rct value increased reaching 932 ohm. After immobilization of the aptamer on the electrode, a semi-circle with fairly large diameter was monitored. The observed increase in the value of Rct was attributed to the electron transfer hindrance by the negatively charged aptamer.

Target Detection and Calibration modeling for DCL

The detection of DCL was carried out by incubating the aptamer-modified electrode with DCL solutions at different concentrations. The performances of the aptasensor was investigated by recording its EIS responses in 0.1 M PBS containing 5 mM $[Fe(CN)_6]^{3-/4-}$ solution.

As illustrated in Figure 10, when the DCL concentration increases Rct decreases. This can be attributed to the change in the spatial conformation of the aptamer in contact with higher concentrations of DCL. The results show that the negative charge density on the surface is lowered due to such conformational changes. Therefore there is a decrease in the interfacial charge transfer resistance to the negatively charged redox probe [29].

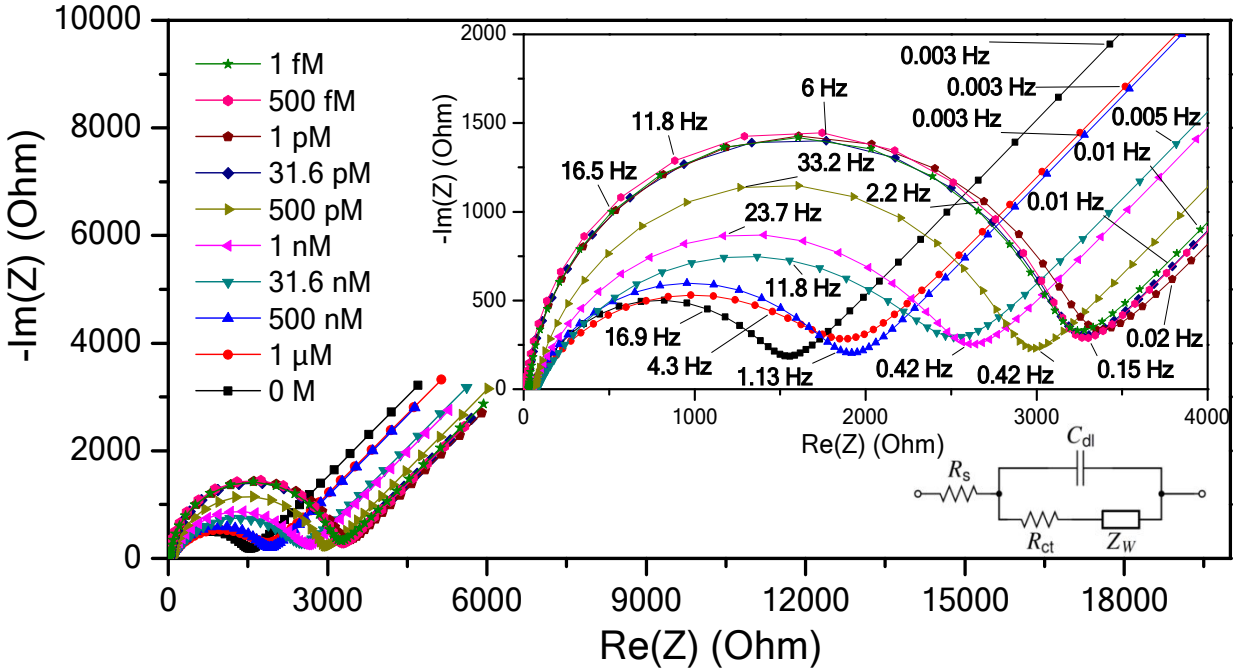

Figure 10. Nyquist plot obtained in 0.1 M PBS containing 5 mM $K_4[Fe(CN)_6]$ and $K_3[Fe(CN)_6]$ after treatment of the aptasensor with different concentrations of DCL in the frequency range of 100 kHz to 1 mHz.

The change in charge-transfer resistance (Fig. 10) was found to be linear with target concentration in the range of 30 pM to 1 μM. A good linear relationship between Rct and DCL concentration was obtained (R^2 = 0.9787), according to the following equation:

Rct= – 310.23 [DCL] – 99.637. The detection limit was calculated to be 0.02 nM from the intersection between the linear part and the non-sensitive linear region (Fig. 11).

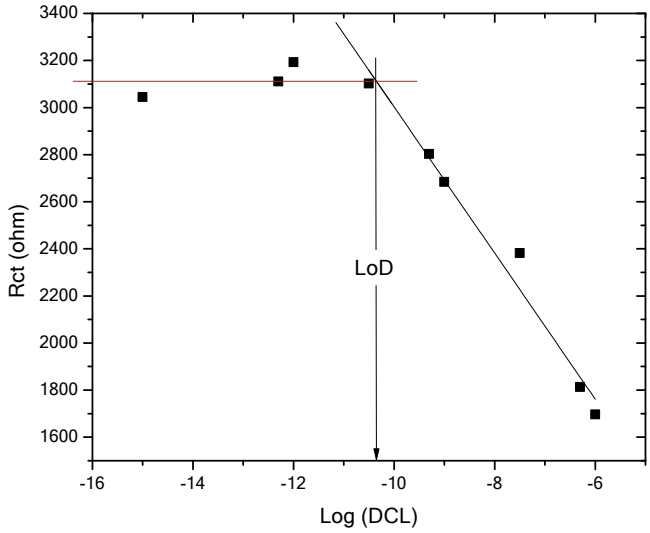

Figure 11. Calibration curve using Rct *vs*. Log DCL concentration

Stability and Reproducibility Study

Once the response of the sensor to DCL demonstrated, the stability and reproducibility merits of the protocol developed were evaluated. The operational stability and performance of the developed aptasensor was assessed for a long-term storage at 4°C using five different electrodes modified with aptamers. The impedance response of the aptasensor was evaluated and it was observed that the aptasensor retained 95.6 % of its initial response after 7 days storage and 92.3 % after 14 days storage (detection of 500 pM of DCL), indicating a good stability.

Furthermore, in order to evaluate the reproducibility of the aptasensor, five aptasensors were treated with 500 pM DCL, and Rct was recorded in 0.1M PBS containing 5mM $[Fe(CN)_6]^{3-/4-}$. The relative

standard deviation (RSD) of their response was found to be 4.8 %. This shows that the reproducibility of the aptasensor is quite reliable. The reproducibility of the different stages of electrode construction was also evaluated (Figure 12). The observed variations can be explained by the several uncontrolled factors that can affect the impedimetric results as the electrodes are handmade.

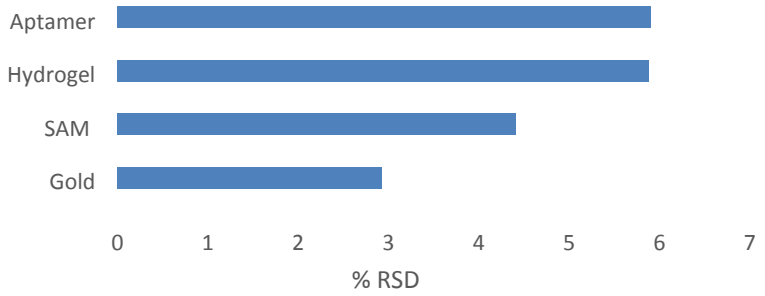

Figure 12. Relative standard deviation of the recorded electron transfer resistance (Rct) of different stages of electrode construction in 0.1M PBS containing 5mM $[Fe(CN)_6]^{3-/4-}$ for five different aptasensors.

Comparative Data

As mentioned above, several electroanalytical methods have been reported for the determination of DCL based on potentiometry, differential pulse voltammetry, square wave voltammetry, linear sweep voltammetry, photo electrochemical and electrochemical impedance spectroscopy. The LOD reached with most of these techniques are not lower than a few tens of nanomole L^{-1}.

Improvement of target detection at the transducing surface using biomolecules specific for DCL have been tried before and published using nucleic acid aptamers. In this regard, the latest improved LOD (in the nM range) achieved for detection of DCL using aptamers is the one demonstrated by Derikvand *et al.* [54], using nanostructured electrodes. To the best of our knowledge, there are no reports on utilization of surface-attached hydrogel films for improved immobilization of aptamer and hence an increased detection of DCL using electrochemical methods, which is the focus of the present study. The figure of merits of different electrochemical methods for detection of DCL are summarized in Table 1, and compared with the previous reports for the determination of DCL. Our proposed method has obviously the best limit of detection and sensitivity for DCL analysis.

Detection method	Modifier	Linear range	LOD	Refs.
Potentiometry	Membrane containing β -cyclodextrin coupled with magnetite ferric oxide (CV-Fe(beta-CD))	10 μM to 10 mM	$11x10^3$ nM	36
Photoelectrochemical (PEC)	DCL Aptamer/Gold nanoparticles (Au NPs) and graphene-doped CdS (GR-CdS)(Au/GR-CdS/Aptamer)	1 to 150 nM	0.78 nM	67
Differential Pulse Voltammetry (DPV)	Functionalized multi-walled carbon nanotubes (f-MWCNTs) and gold-platinum bimetallic nanoparticles (Au-PtNPs) (Au-PtNPs/fMWCNTs/Au)	0.5 to 1000 μM	300 nM	68
Electrochemical Impedance Spectroscopy (EIS)	DCL Aptamer immobilized on the surface of the glassy carbon electrode (GCE)(GCE/AHA/Aptamer)	0 – 5 μM ;10 μM to 1 mM	270 nM	29
Differential Pulse Voltammetry (DPV)	A diclofenac (DCL) imprinted polymer	16.8 to 270 μM	$3.72x10^3$ nM	23
Electrochemical Impedance Spectroscopy (EIS)	Platinum nanoparticles (PtNPs) on carbon nanotubes (CNTs) functionalized with polyethyleneimine (PEI) (PtNPs/PEI/CNTs/Aptamer)	10 to 200 nM	2.7 nM	54

Linear Sweep Voltammetry (LSV)	A multi-walled carbon nanotubes (MWNTs)-dihexadecyl hydrogen phosphate (DHP) film-coated glassy carbon electrode (MWNTs-DHP/GCE)	0.17 to 2.5 μM	80 nM	31
Potentiometry	Modified graphite pencil electrode (MGPE) with doped polypyrrole films (MGPE/ PPy-DCL)	310 μM to11 mM	$190x10^3$ nM	34
Differential Pulse Voltammetry (DPV)	Multiwalled carbon nanotube and ionic liquid modified carbon ceramic electrode (MWCNT-IL/CCE)	0.05 to 50 μM	18 nM	38
Electrochemical Impedance Spectroscopy (EIS)	Aptamer immobilized on the Surface of hydrogel matrix modified gold electrode (Au/SAM/hydrogel/Aptamer)	30 pM to 1 μM	0.02 nM	This work

Table1. Comparison between analytical performances of reported techniques for DCL detection.

CONCLUSION

This study shows an electrochemical impedance spectroscopy biosensor for DCL detection with high sensitivity. Surface-attached hydrogel film with controlled architecture was fabricated as immobilization matrix and was finely characterized. The electrochemical properties of the biosensor in different media and its stability were then studied. The recognition of DCL by the aptamer-based electrode results in an electron transfer resistance change for the $[Fe(CN)_6]^{3-/4-}$ as probed by the EIS technique. The addition of DCL shows a linear change in charge-transfer resistance with the target concentration. EIS aptasensor for DCL with nano molar detection limit was evidenced. The stability and reproducibility of the biosensor were also proved. The aptasensor designed provides a platform for simple, selective and more importantly rapid detection of DCL. The sensing platforms can serve molecular recognition of different targets in the field of health, or in the field of environment. Furthermore, increased sensitivity and specificity can be achieved by incorporating nanostructured metallic materials like gold nanoparticles inside the hydrogel network.

Corresponding Authors

*Dr. Cyrine Slim (cyrine.slim@chimieparistech.psl.eu)

*Dr. Yvette Tran (yvette.tran@espci.fr)

Author Contributions

The manuscript was written through contributions of all authors. All authors have given approval to the final version of the manuscript.

ACKNOWLEDGMENT

We gratefully thank PSL ("Investissements d'avenir", program ANR-10-IDEX-0001-02 PSL), French embassy and Ethiopian Ministry of education (PhD program Ethio-France). We would likewise to extend our gratitude to Dr Grégory Lefèvre from "Institut de Recherche de Chimie Paris" (IRCP) - Chimie ParisTech for his help on the ATR-FTIR measurements.

This work has received the support of Institute Pierre-Gilles de Gennes (équipement d'excellence, "Investissements d'avenir", program ANR-10-EQPX-0034).

ABBREVIATIONS

AFM, Atomic Force Microscopy; ATR-FTIR, Attenuated total reflectance-Fourier transform infrared spectroscopy; BWB, Binding Washing Buffer; Cdl, double-layer capacitance; CLAG, Cross-Linking And Grafting; CV, Cyclic Voltammetry; DCL, Diclofenac; DTE, 1,4-dithioerythritol; EDC, 1-ethyl-3-(3-dimethylaminopropyl) carbodiimide; EIS, Electrochemical Impedance Spectroscopy; GC, Gas chromatography; HPLC, High-performance liquid

chromatography; LOD, limit of detection; MS, Mass spectroscopy; NHS, N-hydroxysuccinimide; PAA, Poly (acrylic acid); Rct, electron transfer resistance; SCE, Saturated Calomel Electrode; SEM, Scanning Electron Microscopy; WCA, Water Contact Angle.

Supporting Information

Fabrication steps of the Electrode using photolithography process, cleaning procedure and surface characterization.

REFERENCES

(1) Solomon, D. H.; Avorn, J.; Stürmer, T.; Glynn, R. J.; Mogun, H.; Schneeweiss, S. Cardiovascular Outcomes in New Users of Coxibs and Nonsteroidal Antiinflammatory Drugs: High-Risk Subgroups and Time Course of Risk. *Arthritis Rheum.* **2006**, *54* (5), 1378–1389. https://doi.org/10.1002/art.21887.

(2) Tiedeken, E. J.; Tahar, A.; McHugh, B.; Rowan, N. J. Monitoring, Sources, Receptors, and Control Measures for Three European Union Watch List Substances of Emerging Concern in Receiving Waters – A 20 Year Systematic Review. *Sci. Total Environ.* **2017**, *574*, 1140–1163. https://doi.org/10.1016/j.scitotenv.2016.09.084.

(3) Altman, R.; Bosch, B.; Brune, K.; Patrignani, P.; Young, C. Advances in NSAID development: evolution of diclofenac products using pharmaceutical technology, Drugs **2015**, 75, 859–877. https://doi.org/10.1007/s40265-015-0392-z.

(4) Gan, T. J. Diclofenac: an update on its mechanism of action and safety profile, Curr. Med. Res. Opin. **2010**, 26, 1715–1731. https://doi.org/10.1185/03007995.2010.486301.

(5) Paíga, P.; Santos, L. H. M. L. M.; Ramos, S.; Jorge, S.; Silva, J. G.; Delerue-Matos, C. Presence of pharmaceuticals in the Lis river (Portugal): sources, fate and seasonal variation, Sci. Total Environ. **2016**, 573, 164–177. https://doi.org/10.1016/j.scitotenv.2016.08.089.

(6) Lonappan, L.; Brar, S. K.; Das, R. K.; Verma, M.; Surampalli, R. Y. Diclofenac and its transformation products: environmental occurrence and toxicity - a review, Environ. Int. **2016**, 96, 127–138. https://doi.org/10.1016/j.envint.2016.09.014.

(7) Zhang, Y.; Geißen, S.U.; Gal, C. Carbamazepine and diclofenac: removal in waste water treatment plants and occurrence in water bodies, Chemosphere **2008**, 73, 1151–1161. https://doi.org/10.1016/j.chemosphere.2008.07.086.

(8) Petrie, B.; Barden, R.; Kasprzyk-Hordern, B. A review on emerging contaminants in wastewaters and the environment: current knowledge, understudied areas and recommendations for future monitoring, Water Res. **2014**, 72, 3–27. https://doi.org/10.1016/j.watres.2014.08.053.

(9) Richardson, S. D.; Ternes, T. A. Water analysis: emerging contaminants and current issues, Anal. Chem. **2014**, 86, 2813 – 2848. https://doi.org/10.1021/ac500508t.

(10) Albero, B.; Sanchez-Brunete, C.; García-Valcarcel, A. I.; Perez, R. A.; Tadeo, J. L. Ultrasound-assisted extraction of emerging contaminants from environmental samples, TrAC Trends Anal. Chem. **2015**, 71, 110 – 118. https://doi.org/10.1016/j.trac.2015.03.015.

(11) Sui, Q.; Cao, X.; Lu, S.; Zhao, W.; Qiu, Z.; Yu, G. Occurrence, sources and fate of pharmaceuticals and personal care products in the ground water: a review, Emerg. Contam. **2015**, 1, 14 – 24. https://doi.org/10.1016/j.emcon.2015.07.001.

(12) Luo, Y.; Guo, W.; Ngo, H. H.; Nghiem, L. D.; Hai, F. I.; Zhang, J.; Liang, S.; Wang, X. C. A review on the occurrence of micropollutants in the aquatic environment and their fate and removal during wastewater treatment, Sci. Total Environ. **2014**, 473–474, 619–641. https://doi.org/10.1016/j.scitotenv.2013.12.065.

(13) Hoeger, B.; Köllner, B.; Dietrich, D. R.; Hitzfeld, B. Water-borne diclofenac affects kidney and gill integrity and selected immune parameters in brown trout (Salmo trutta f. fario), Aquat. Toxicol. **2005**, 75, 53 – 64. https://doi.org/10.1016/j.aquatox.2005.07.006.

(14) Triebskorn, R.; Casper, H.; Scheil, V. J. Schwaiger, Ultrastructural effects of pharmaceuticals (carbamazepine, clofibric acid, metoprolol, diclofenac) in rainbow trout (Oncorhynchus mykiss) and common carp (Cyprinus carpio), Anal. Bioanal. Chem. **2007**, 387, 1405–1416. https://doi.org/10.1007/s00216-006-1033-x.

(15) Ebele, A. J.; Abou-Elwafa Abdallah, M.; Harrad, S.; Pharmaceuticals and personal care products (PPCPs) in the freshwater aquatic environment, Emerg. Contam. **2017**, 3, 1–16. https://doi.org/10.1016/j.emcon.2016.12.004.

(16) Cleuvers, M. Mixture Toxicity of the Anti-Inflammatory Drugs Diclofenac, Ibuprofen, Naproxen, and Acetylsalicylic Acid. *Ecotoxicol. Environ. Saf.* **2004**, *59* (3), 309–315. https://doi.org/10.1016/S0147-6513(03)00141-6.

(17) Arcelloni, C.; Lanzi, R.; Pedercini, S.; Molteni, G.; Fermo, I.; Pontiroli, A.; Paroni, R. High-Performance Liquid Chromatographic Determination of Diclofenac in Human Plasma after Solid-Phase Extraction. *J. Chromatogr. B. Biomed. Sci. App.* **2001**, *763* (1–2), 195–200. https://doi.org/10.1016/S0378-4347(01)00383-8.

(18) Yilmaz, B.; Asci, A.; Palabiyik, S. S. HPLC Method for Determination of Diclofenac in Human Plasma and Its Application to a Pharmacokinetic Study in Turkey. *J. Chromatogr. Sci.* **2011**, *49* (6), 422–427. https://doi.org/10.1093/chrsci/49.6.422.

(19) Auroux, P.-A.; Iossifidis, D.; Reyes, D. R.; Manz, A. Micro Total Analysis Systems. 2. Analytical Standard Operations and Applications. *Anal. Chem.* **2002**, *74* (12), 2637–2652. https://doi.org/10.1021/ac020239t.

(20) Karimi-Maleh, H.; Biparva, P.; Hatami, M. A Novel Modified Carbon Paste Electrode Based on NiO/CNTs Nanocomposite and (9, 10-Dihydro-9, 10-Ethanoanthracene-11, 12-Dicarboximido)-4-Ethylbenzene-1, 2-Diol as a Mediator for Simultaneous Determination of Cysteamine, Nicotinamide Adenine Dinucleotide and Folic Acid. *Biosens. Bioelectron.* **2013**, *48*, 270–275. https://doi.org/10.1016/j.bios.2013.04.029.

(21) Ensafi, A. A.; Karimi-Maleh, H.; Mallakpour, S.; Hatami, M. Simultaneous Determination of N-Acetylcysteine and Acetaminophen by Voltammetric Method Using N-(3,4-Dihydroxyphenethyl)-3,5-Dinitrobenzamide Modified Multiwall Carbon Nanotubes Paste Electrode. *Sens. Actuators B Chem.* **2011**, *155* (2), 464–472. https://doi.org/10.1016/j.snb.2010.12.048.

(22) Sanghavi, B. J.; Mobin, S. M.; Mathur, P.; Lahiri, G. K.; Srivastava, A. K. Biomimetic Sensor for Certain Catecholamines Employing Copper(II) Complex and Silver Nanoparticle Modified Glassy Carbon Paste Electrode. *Biosens. Bioelectron.* **2013**, *39* (1), 124–132. https://doi.org/10.1016/j.bios.2012.07.008.

(23) Mostafavi, M.; Yaftian, M. R.; Piri, F.; Shayani-Jam, H. A New Diclofenac Molecularly Imprinted Electrochemical Sensor Based upon a Polyaniline/Reduced Graphene Oxide Nano-Composite. *Biosens. Bioelectron.* **2018**, *122*, 160–167. https://doi.org/10.1016/j.bios.2018.09.047.

(24) Lenik, J. A New Potentiometric Electrode Incorporating Functionalized β-Cyclodextrins for Diclofenac Determination. *Mater. Sci. Eng. C* **2014**, *45*, 109–116. https://doi.org/10.1016/j.msec.2014.08.072.

(25) Wang, C.; Jiang, T.; Zhao, K.; Deng, A.; Li, J. A Novel Electrochemiluminescent Immunoassay for Diclofenac Using Conductive Polymer Functionalized Graphene Oxide as Labels and Gold Nanorods as Signal Enhancers. *Talanta* **2019**, *193*, 184–191. https://doi.org/10.1016/j.talanta.2018.09.103.

(26) Wang, S.; Liu, Q.; Li, H.; Li, Y.; Hao, N.; Qian, J.; Zhu, W.; Wang, K. Fabrication of Label-Free Electrochemical Impedimetric DNA Biosensor for Detection of Genetically Modified

Soybean by Recognizing CaMV 35S Promoter. *J. Electroanal. Chem.* **2016**, *782*, 19–25. https://doi.org/10.1016/j.jelechem.2016.09.052.

(27) Asif, M.; Aziz, A.; Azeem, M.; Wang, Z.; Ashraf, G.; Xiao, F.; Chen, X.; Liu, H. A Review on Electrochemical Biosensing Platform Based on Layered Double Hydroxides for Small Molecule Biomarkers Determination. *Adv. Colloid Interface Sci.* **2018**, *262*, 21–38. https://doi.org/10.1016/j.cis.2018.11.001.

(28) Sanati, A. L.; Karimi-Maleh, H.; Badiei, A.; Biparva, P.; Ensafi, A. A. A Voltammetric Sensor Based on NiO/CNTs Ionic Liquid Carbon Paste Electrode for Determination of Morphine in the Presence of Diclofenac. *Mater. Sci. Eng. C* **2014**, *35*, 379–385. https://doi.org/10.1016/j.msec.2013.11.031.

(29) Kashefi-Kheyrabadi, L.; Mehrgardi, M. A. Design and Construction of a Label Free Aptasensor for Electrochemical Detection of Sodium Diclofenac. *Biosens. Bioelectron.* **2012**, *33* (1), 184–189. https://doi.org/10.1016/j.bios.2011.12.050.

(30) Rodríguez, J. A.; Barrado, E.; Castrillejo, Y.; Santos, J. R.; Lima, J. L. F. C. Validation of a Tubular Bismuth Film Amperometric Detector. *J. Pharm. Biomed. Anal.* **2007**, *45* (1), 47–53. https://doi.org/10.1016/j.jpba.2007.05.025.

(31) Yang, X.; Wang, F.; Hu, S. Enhanced Oxidation of Diclofenac Sodium at a Nano-Structured Electrochemical Sensing Film Constructed by Multi-Wall Carbon Nanotubes–Surfactant Composite. *Mater. Sci. Eng. C* **2008**, *28* (1), 188–194. https://doi.org/10.1016/j.msec.2006.11.006.

(32) Hajjizadeh, M.; Jabbari, A.; Heli, H.; Moosavi-Movahedi, A. A.; Haghgoo, S. Electrocatalytic Oxidation of Some Anti-Inflammatory Drugs on a Nickel Hydroxide-

Modified Nickel Electrode. *Electrochimica Acta* **2007**, *53* (4), 1766–1774. https://doi.org/10.1016/j.electacta.2007.08.026.

(33) Daneshgar, P.; Norouzi, P.; Ganjali, M.; Dinarvand, R.; Moosavi-Movahedi, A. Determination of Diclofenac on a Dysprosium Nanowire- Modified Carbon Paste Electrode Accomplished in a Flow Injection System by Advanced Filtering. *Sensors* **2009**, *9* (10), 7903–7918. https://doi.org/10.3390/s91007903.

(34) Oliveira, M. C.; Bindewald, E. H.; Marcolino, L. H.; Bergamini, M. F. Potentiometric Determination of Diclofenac Using an Ion-Selective Electrode Prepared from Polypyrrole Films. *J. Electroanal. Chem.* **2014**, *732*, 11–16. https://doi.org/10.1016/j.jelechem.2014.08.006.

(35) Kormosh, Zh. A.; Hunka, I. P.; Bazel, Ya. R. A Potentiometric Sensor for the Determination of Diclofenac. *J. Anal. Chem.* **2009**, *64* (8), 853–858. https://doi.org/10.1134/S1061934809080140.

(36) Elbalkiny, H. T.; Yehia, A. M.; Riad, S. M.; Elsaharty, Y. S. Potentiometric Diclofenac Detection in Wastewater Using Functionalized Nanoparticles. *Microchem. J.* **2019**, *145*, 90–95. https://doi.org/10.1016/j.microc.2018.10.017.

(37) Manea, F.; Ihos, M.; Remes, A.; Burtica, G.; Schoonman, J. Electrochemical Determination of Diclofenac Sodium in Aqueous Solution on Cu-Doped Zeolite-Expanded Graphite-Epoxy Electrode. *Electroanalysis* **2010**, *22* (17–18), 2058–2063. https://doi.org/10.1002/elan.201000074.

(38) Sarhangzadeh, K.; Khatami, A. A.; Jabbari, M.; Bahari, S. Simultaneous Determination of Diclofenac and Indomethacin Using a Sensitive Electrochemical Sensor Based on

Multiwalled Carbon Nanotube and Ionic Liquid Nanocomposite. *J. Appl. Electrochem.* **2013**, *43* (12), 1217–1224. https://doi.org/10.1007/s10800-013-0609-3.

(39) Karuppiah, C.; Cheemalapati, S.; Chen, S.-M.; Palanisamy, S. Carboxyl-Functionalized Graphene Oxide-Modified Electrode for the Electrochemical Determination of Nonsteroidal Anti-Inflammatory Drug Diclofenac. *Ionics* **2015**, *21* (1), 231–238. https://doi.org/10.1007/s11581-014-1161-9.

(40) Huebner, M.; Weber, E.; Niessner, R.; Boujday, S.; Knopp, D. Rapid Analysis of Diclofenac in Freshwater and Wastewater by a Monoclonal Antibody-Based Highly Sensitive ELISA. *Anal. Bioanal. Chem.* **2015**, *407* (29), 8873–8882. https://doi.org/10.1007/s00216-015-9048-9.

(41) Hlaváček, A.; Farka, Z.; Hübner, M.; Horňáková, V.; Němeček, D.; Niessner, R.; Skládal, P.; Knopp, D.; Gorris, H. H. Competitive Upconversion-Linked Immunosorbent Assay for the Sensitive Detection of Diclofenac. *Anal. Chem.* **2016**, *88* (11), 6011–6017. https://doi.org/10.1021/acs.analchem.6b01083.

(42) Hayat, A.; Marty, J. L. Aptamer Based Electrochemical Sensors for Emerging Environmental Pollutants. *Front. Chem.* **2014**, *2*. https://doi.org/10.3389/fchem.2014.00041.

(43) Joeng, C. B.; Niazi, J. H.; Lee, S. J.; Gu, M. B. SsDNA Aptamers That Recognize Diclofenac and 2-Anilinophenylacetic Acid. *Bioorg. Med. Chem.* **2009**, *17* (15), 5380–5387. https://doi.org/10.1016/j.bmc.2009.06.044.

(44) Strehlitz, B.; Reinemann, C.; Linkorn, S.; Stoltenburg, R. Aptamers for Pharmaceuticals and Their Application in Environmental Analytics. *Bioanal. Rev.* **2012**, *4* (1), 1–30. https://doi.org/10.1007/s12566-011-0026-1.

(45) Radom, F.; Jurek, P. M.; Mazurek, M. P.; Otlewski, J.; Jele?, F. Aptamers: Molecules of Great Potential. *Biotechnol. Adv.* **2013**, *31* (8), 1260–1274. https://doi.org/10.1016/j.biotechadv.2013.04.007.

(46) Balamurugan, S.; Obubuafo, A.; Soper, S. A.; McCarley, R. L.; Spivak, D. A. Designing Highly Specific Biosensing Surfaces Using Aptamer Monolayers on Gold. *Langmuir* **2006**, *22* (14), 6446–6453. https://doi.org/10.1021/la060222w.

(47) Tombelli, S.; Minunni, M.; Mascini, M. Analytical Applications of Aptamers. *Biosens. Bioelectron.* **2005**, *20* (12), 2424–2434. https://doi.org/10.1016/j.bios.2004.11.006.

(48) Hamula, C.; Guthrie, J.; Zhang, H.; Li, X.; Le, X. Selection and Analytical Applications of Aptamers. *TrAC Trends Anal. Chem.* **2006**, *25* (7), 681–691. https://doi.org/10.1016/j.trac.2006.05.007.

(49) Tom, S.; Jin, H.-E.; Lee, S.-W. Aptamers as Functional Bionanomaterials for Sensor Applications. In *Engineering of Nanobiomaterials*; Elsevier, 2016; pp 181–226. https://doi.org/10.1016/B978-0-323-41532-3.00006-3.

(50) Menger, M.; Glökler, J.; Rimmele, M. Application of Aptamers in Therapeutics and for Small-Molecule Detection. In *RNA Towards Medicine*; Erdmann, V., Barciszewski, J., Brosius, J., Eds.; Springer-Verlag: Berlin/Heidelberg, 2006; Vol. 173, pp 359–373. https://doi.org/10.1007/3-540-27262-3_18.

(51) Nguyen, V.-T.; Kwon, Y. S.; Gu, M. B. Aptamer-Based Environmental Biosensors for Small Molecule Contaminants. *Curr. Opin. Biotechnol.* **2017**, *45*, 15–23. https://doi.org/10.1016/j.copbio.2016.11.020.

(52) Hayat, A.; Haider, W.; Rolland, M.; Marty, J.-L. Electrochemical Grafting of Long Spacer Arms of Hexamethyldiamine on a Screen Printed Carbon Electrode Surface: Application in

Target Induced Ochratoxin A Electrochemical Aptasensor. *The Analyst* **2013**, *138* (10), 2951. https://doi.org/10.1039/c3an00158j.

(53) Hayat, A.; Andreescu, S.; Marty, J.-L. Design of PEG-Aptamer Two Piece Macromolecules as Convenient and Integrated Sensing Platform: Application to the Label Free Detection of Small Size Molecules. *Biosens. Bioelectron.* **2013**, *45*, 168–173. https://doi.org/10.1016/j.bios.2013.01.059.

(54) Derikvand, H.; Roushani, M.; Abbasi, A. R.; Derikvand, Z.; Azadbakht, A. Design of Folding-Based Impedimetric Aptasensor for Determination of the Nonsteroidal Anti-Inflammatory Drug. *Anal. Biochem.* **2016**, *513*, 77–86. https://doi.org/10.1016/j.ab.2016.06.013.

(55) Feng, L.; Wang, L.; Hu, Z.; Tian, Y.; Xian, Y.; Jin, L. Encapsulation of Horseradish Peroxidase into Hydrogel, and Its Bioelectrochemistry. *Microchim. Acta* **2009**, *164* (1–2), 49–54. https://doi.org/10.1007/s00604-008-0030-5.

(56) Chollet, B.; Li, M.; Martwong, E.; Bresson, B.; Fretigny, C.; Tabeling, P.; Tran, Y. Multiscale Surface-Attached Hydrogel Thin Films with Tailored Architecture. *ACS Appl. Mater. Interfaces* **2016**, *8* (18), 11729–11738. https://doi.org/10.1021/acsami.6b00446.

(57) Li, M.; Bresson, B.; Cousin, F.; Fretigny, C.; Tran, Y. Submicrometric Films of Surface-Attached Polymer Network with Temperature-Responsive Properties. *Langmuir* **2015**, *31* (42), 11516–11524. https://doi.org/10.1021/acs.langmuir.5b02948.

(58) Miquelard-Garnier, G.; Demeures, S.; Creton, C.; Hourdet, D. Synthesis and Rheological Behavior of New Hydrophobically Modified Hydrogels with Tunable Properties. *Macromolecules* **2006**, *39* (23), 8128–8139. https://doi.org/10.1021/ma061361n.

(59) Chang, S. C.; Chao, I.; Tao, Y.-T. Structures of Self-Assembled Monolayers of Aromatic-Derivatized Thiols on Evaporated Gold and Silver Surfaces: Implication on Packing Mechanism. J. Am.Chem.Soc.**1994**, 116, 6792-6805.

(60) Laibinis, P. E.; Parikh, A. N.; Nuzzo, R. G. Comparison of the Structures and Wetting Properties of Self-Assembled Monolayers of n-Alkanethiols on the Coinage Metal Surfaces, Cu, Ag, Au. J.Am.Chem.Soc.**1991**,113,7152-7167.

(61) Yadav, V.; Harkin, A. V.; Robertson, M. L.; Conrad, J. C. Hysteretic Memory in PH-Response of Water Contact Angle on Poly(Acrylic Acid) Brushes. *Soft Matter* **2016**, *12* (15), 3589–3599. https://doi.org/10.1039/C5SM03134F.

(62) Mendes, R. K.; Freire, R. S.; Fonseca, C. P.; Neves, S.; Kubota, L. T. Characterization of Self-Assembled Thiols Monolayers on Gold Surface by Electrochemical Impedance Spectroscopy. *J. Braz. Chem. Soc.* **2004**, *15* (6), 849–855. https://doi.org/10.1590/S0103-50532004000600011.

(63) Azzaroni, O.; Vela, M. E.; Martin, H.; Hernández Creus, A.; Andreasen, G.; Salvarezza, R. C. Electrodesorption Kinetics and Molecular Interactions at Negatively Charged Self-Assembled Thiol Monolayers in Electrolyte Solutions. *Langmuir* **2001**, *17* (21), 6647–6654. https://doi.org/10.1021/la010019v.

(64) Sudre, G.; Hourdet, D.; Creton, C.; Cousin, F.; Tran, Y. PH-Responsive Swelling of Poly(Acrylic Acid) Brushes Synthesized by the Grafting Onto Route. *Macromol. Chem. Phys.* **2013**, *214* (24), 2882–2890. https://doi.org/10.1002/macp.201300477.

(65) Lego, B.; Skene, W. G.; Giasson, S. Swelling Study of Responsive Polyelectrolyte Brushes Grafted from Mica Substrates: Effect of PH, Salt, and Grafting Density. *Macromolecules* **2010**, *43* (9), 4384–4393. https://doi.org/10.1021/ma902588j.

(66) Alfonta, L.; Bardea, A.; Khersonsky, O.; Katz, E.; Willner, I. Chronopotentiometry and Faradaic Impedance Spectroscopy as Signal Transduction Methods for the Biocatalytic Precipitation of an Insoluble Product on Electrode Supports: Routes for Enzyme Sensors, Immunosensors and DNA Sensors. *Biosens. Bioelectron.* **2001**, *16* (9–12), 675–687. https://doi.org/10.1016/S0956-5663(01)00231-7.

(67) Okoth, O. K.; Yan, K.; Feng, J.; Zhang, J. Label-Free Photoelectrochemical Aptasensing of Diclofenac Based on Gold Nanoparticles and Graphene-Doped CdS. *Sens. Actuators B Chem.* **2018**, *256*, 334–341. https://doi.org/10.1016/j.snb.2017.10.089

.

(68) Eteya, M. M.; Rounaghi, G. H.; Deiminiat, B. Fabrication of a New Electrochemical Sensor Based on Au Pt Bimetallic Nanoparticles Decorated Multi-Walled Carbon Nanotubes for Determination of Diclofenac. *Microchem. J.* **2019**, *144*, 254–260. https://doi.org/10.1016/j.microc.2018.09.009.
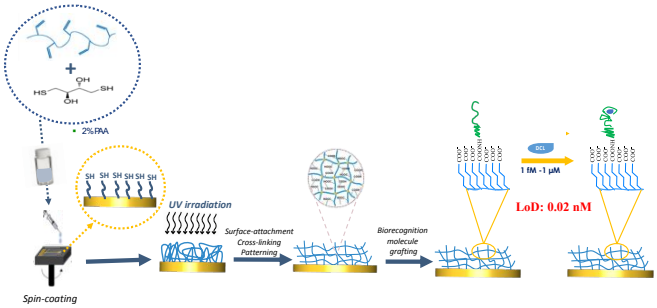
For Table of Contents Use Only